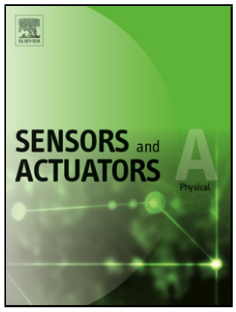

Title: Wideband MEMS Resonator Using Multifrequency Excitation

Author: N. Jaber A. Ramini Q. Hennawi M.I. Younis

PII: S0924-4247(16)30085-1
DOI: http://dx.doi.org/doi:10.1016/j.sna.2016.02.030
Reference: SNA 9541

To appear in: *Sensors and Actuators A*

Received date: 3-11-2015
Revised date: 8-2-2016
Accepted date: 15-2-2016

Please cite this article as: N.Jaber, A.Ramini, Q.Hennawi, M.I.Younis, Wideband MEMS Resonator Using Multifrequency Excitation, Sensors and Actuators: A Physical http://dx.doi.org/10.1016/j.sna.2016.02.030

Wideband MEMS Resonator Using Multifrequency Excitation

N. Jaber,[1] A. Ramini,[1] Q. Hennawi,[1] and M. I. Younis[1,2,a]

[1]*Physical Science and Engineering Division, King Abdullah University of Science and Technology, Thuwal, 23955-6900, Saudi Arabia*

[2]*Department of Mechanical Engineering, State University of New York, Binghamton, NY 13902, USA*

[a] Corresponding author Electronic mail: Mohammad.Younis@kaust.edu.sa

Highlights

- The motivation of this study is to demonstrate the ability to excite the combination resonances near the first and third mode of vibration of clamped-clamped microbeams fabricated using surface micromachining techniques.
- The ability to control the resonator bandwidth and the amplitude of vibration is demonstrated experimentally, by controlling the amplitude and frequency of the electrical excitation force.
- This ability to excite multiple peaks and to control the resonator's bandwidth has promising applications in mass sensing and energy harvesting applications.
- Another objective is to explore the dynamics of out-of-plane structures made of Polyimide, which is bio-compatible material. The surface of these microbeams can be functionalized with polymers and other sorbent materials to allow mass/gas detection. The information about the use of such material is scarce and is not available for the science community.
- The final objective of this work is to study in details, the frequency response of these devices at the higher-order modes up to the nonlinear regime. Our study has shown interesting jumps and hardening effects at the higher-order modes.

ABSTRACT

We demonstrate the excitation of combination resonances of additive and subtractive types and their exploitations to realize a large bandwidth micro-machined resonator of large amplitude even at higher harmonic modes of vibrations. The investigation is conducted on a Microelectromechanical systems (MEMS) clamped-clamped microbeam fabricated using polyimide as a structural layer coated with nickel from top and chromium and gold layers from bottom. The microbeam is excited by a two-source harmonic excitation, where the first frequency source is swept around the targeted resonance (first or third mode of vibration) while the second source frequency is kept fixed. We report for the first time a large bandwidth and large amplitude response near the higher order modes of vibration. Also, we show that by properly tuning the frequency and amplitude of the excitation force, the frequency bandwidth of the resonator is controlled.

1. Introduction

There is a growing demand to develop tunable resonators with wide frequency band especially at high quality factor range and near higher-order modes of vibrations, where high sensitivity is demanded for gyroscopes [1], energy harvesting [2, 3], filtering [4-6], logic gates [7-9], and electron sensing applications [10].

MEMS gyroscopes rely on exiting a resonator at the maximum peak at resonance for both the driving and sensing modes to achieve the highest possible dynamic response, and hence, maximize the sensitivity [1, 11]. Maximizing the peak response means that the quality factor of the resonator should be maximized. However, this leads to reduction in the frequency bandwidth of high power and large response. Therefore, practically, due to fabrication imperfections, noise, and temperature drift problems, catching exactly the maximum peak becomes almost impossible resulting in significant loss of sensitivity. To alleviate this effect and to broaden the bandwidth at resonance, mechanically coupled resonators were proposed in the driving mode, the sensing mode, and in both [1].

To harvest the maximum energy from the ambient vibration, the harvester resonant frequency is designed to match the ambient vibration frequency. Any deviation between the two frequencies causes significant decrease in the harvested power. Zhu *et al.* reviewed several strategies to tune and increase the resonator bandwidth for energy harvesting, either by designing complicated resonators or introducing a sophisticated conditioning electrical circuit [2]. These methods require external power to tune the resonator and have limited controllable frequency range [12].

Also, tunable and wide band resonators have been investigated for filtering application in transceivers [6], multiband/multifrequency applications in communication systems [5], and wireless communication including cellular devices [4]. Rhoads *et al.* designed and analytically studied a tunable band pass filter by coupling two parametrically excited MEMS oscillators connected to a logic circuit. They found that using parametric excitation introduces instability problems and might excite higher order resonances, which results in a significant response away from the filter operating range [4]. Piazza *et al.*

designed and fabricated peizoelectrically actuated MEMS resonator composed of rectangular plates and circular rings electrically cascaded in different configurations to form band pass filters at 93 *MHz* and 236 *MHz* [13]. An elctrothermally excited resonator is fabricated and tested in [14]. Using the idea of multifrequency excitation, they showed simultaneous mixing and filtering behavior. To increase the operating frequency range of carbon nanotube resonator, Cho *et al.* exploited the geometric nonlinearities of the resonator excited at high amplitude. The resonance band was increased up to many multiples of the natural frequency [15].

In previous works, we explored multi-frequency excitations of a micro mirror based resonator [16] and a capacitive switch [17]. We showed that due to the inherent quadratic nonlinearity of the electrostatic force, combination resonances can be triggered and tuned depending on the voltage loads amplitude and frequency. The nonlinear dynamics of a clamped-clamped beam resonator when excited by two frequency sources near its first and third resonance frequency (multimodal excitation) has also been investigated theoretically [18]. The complex dynamics of the system has been highlighted through phase diagrams, Poincare sections, bifurcation diagrams, and FFTs showing quasi-periodic bifurcation rout to chaos [18]. Clamped-clamped beams are known to be inherently nonlinear structures due to the cubic nonlinearity of mid-plane stretching, which they suffer from during moderate-large motion. When excited by electrostatic forces, their behavior is influenced by quadratic nonlinearities as well. In this letter, we aim for the first time to exploit these nonlinearities to trigger several combination resonances, which can be tuned and controlled to broaden the bandwidth near resonance and achieve other desirable features.

2. Mathematical model

To illustrate the idea, we recall first that the dynamic response of a linear system excited by several harmonic forces is composed of the same frequency components as the input forcing. For a nonlinear response, however, several other resonances, in addition, can be triggered, including superharmonic, subharmonic, and combination resonances [19, 20]. For an electrically excited clamped-clamped microbeam, for the first approximation, quadratic and cubic nonlinearities can be assumed to be the most dominant nonlinearities of the system [11]. A simple model of this case can be viewed as a single-degree-of-freedom system governing the mid-point deflection of the beam, *u*, with both quadratic and cubic nonlinearities excited by multifrequency harmonic forces, which take the form of

$$\ddot{u}(t) + 2\mu\dot{u}(t) + \omega_0^2 u(t) + \alpha_q u^2(t) + \alpha_c u^3(t) = f(t) \tag{1}$$

where $f(t)$ is the electrical attraction force between the two electrodes:

$$f(t)=\eta V^2(t) \tag{2}$$

where t is time, μ is the damping coefficient, ω_0 is resonance frequency of the system, α_q and α_c are the quadratic and cubic nonlinearities coefficients, respectively, coming from electrostatic and mid-plane stretching, and η is a coefficient related to the projected electrostatic force on the first mode of vibration. The voltage term $V(t)$ is composed of a DC voltage load V_{DC} superimposed to two AC harmonic voltage loads of amplitudes V_{AC1} and V_{AC2} and of frequencies Ω_1 and Ω_2, respectively. Accordingly, the voltage load term, when entering the electrostatic force term, can be expanded as below

$$\begin{aligned} V^2(t)=&\left[V_{DC}+V_{AC1}\cos(\Omega_1 t)+V_{AC2}\cos(\Omega_2 t)\right]^2=\left(V_{DC}^2+\frac{1}{2}V_{AC1}^2+\frac{1}{2}V_{AC2}^2\right)+\left(2V_{DC}V_{AC1}\right)\cos(\Omega_1 t)+\left(2V_{DC}V_{AC2}\right)\cos(\Omega_2 t)\\ &+\left(\frac{1}{2}V_{AC1}^2\right)\cos(2\Omega_1 t)+\left(\frac{1}{2}V_{AC2}^2\right)\cos(2\Omega_2 t)+\left(2V_{AC1}V_{AC2}\right)\cos((\Omega_1+\Omega_2)t)+\left(2V_{AC1}V_{AC2}\right)\cos((\Omega_2-\Omega_1)t)\end{aligned} \tag{3}$$

The excitation frequencies are labeled as $\omega_1=\Omega_1$, $\omega_2=\Omega_2$, $\omega_3=2\Omega_1$, $\omega_4=2\Omega_2$, $\omega_5=\Omega_2+\Omega_1$ and $\omega_6=\Omega_1-\Omega_2$. Next, using the method of straight forward expansion [19] we seek an approximate analytical solution for Eq. (1). Toward this, Eq. (1) is scaled as

$$\ddot{u}(t)+2\varepsilon\mu\dot{u}(t)+\omega_0^2u(t)+\varepsilon\alpha_q u^2(t)+\varepsilon^2\alpha_c u^3(t)=f(t) \tag{4}$$

where ε is scaling parameter. Hence, we seek an expanded solution for u of the form

$$u(t)\approx u_0+\varepsilon u_1+\varepsilon^2 u_2+\cdots \tag{5}$$

Next, we introduce the derivative notations as

$$\begin{aligned}\frac{d}{dt}&=D_0+\varepsilon D_1+\cdots\\ \frac{d^2}{dt^2}&=D_0^2+2\varepsilon D_0D_1+\varepsilon^2(D_1^2+2D_0D_2)+\cdots\end{aligned} \tag{6}$$

Substituting Eq. (5) and Eq. (6) into Eq. (4) and collecting the terms of order ε^0, ε^1 and ε^2 we get

$$O(\varepsilon^0):\ D_0^2u_0+\omega_0^2u_0=\eta V^2(t) \tag{7}$$

$$O(\varepsilon^1):\ D_0^2u_1+\omega_0^2u_1=-2D_0D_1u_0-2\mu D_0u_0-\alpha_q u_0^2 \tag{8}$$

$$O(\varepsilon^2):\ D_0^2u_2+\omega_0^2u_2=-2D_0D_1u_1-D_1^2u_0-2D_0D_2u_0-2\mu D_0u_1-2\mu D_1u_0-2\alpha_q u_0u_1-\alpha_q u_1^2-\alpha_c u_0^3 \tag{9}$$

The solution of Eq. (7) can be written in the form

$$u_0(t) = A(T_1)e^{i\omega_0 T_0} + \sum_{n=1}^{6} \Lambda_n e^{i(\omega_n T_0)} + cc \tag{10}$$

where A is a complex amplitude, $T_0=t$, $T_1=t\varepsilon$, cc denotes the complex conjugate terms, and Λ_n is defined as

$$\Lambda_n = \frac{1}{2}(\omega_0^2 - \omega_n^2)^{-1} \tag{11}$$

Then, substituting Eq. (10) into Eq. (8) and Eq. (9) yields the so-called secular terms [20], which produce several kinds of resonances. Table 1 shows a summary of the most significant triggered resonances by solving Eq. (8). Solving Eq. (9) produces more resonances, for example, the subharmonic of order one third.

TABLE 1. Triggered resonances for a system with quadratic and cubic nonlinearities excited with a multifrequency source.

Frequency	Resonance Type
$\omega_0 \approx \Omega_1, \Omega_2$	Primary
$\omega_0 \approx 2\Omega_1, 2\Omega_2,$ $3\Omega_1, 3\Omega_2, 4\Omega_1, 4\Omega_2$	Superharmonic
$\omega_0 \approx \frac{1}{2}\Omega_1, \frac{1}{2}\Omega_2$	Subharmonic
$\omega_0 \approx \Omega_1 + \Omega_2,$ $\frac{1}{2}(\Omega_1 + \Omega_2), 2(\Omega_1 + \Omega_2)$ $2\Omega_1 + \Omega_2, \Omega_1 + 2\Omega_2$ $\Omega_1 + 3\Omega_2, 3\Omega_1 + \Omega_2$	Combination of sum type
$\omega_0 \approx \Omega_1 - \Omega_2,$ $\Omega_1 - 2\Omega_2, 2\Omega_1 - \Omega_2,$ $\Omega_1 - 3\Omega_2, 3\Omega_1 - \Omega_2$ $2(\Omega_1 - \Omega_2), \frac{1}{2}(\Omega_1 - \Omega_2)$	Combination of difference type

3. Fabrication process

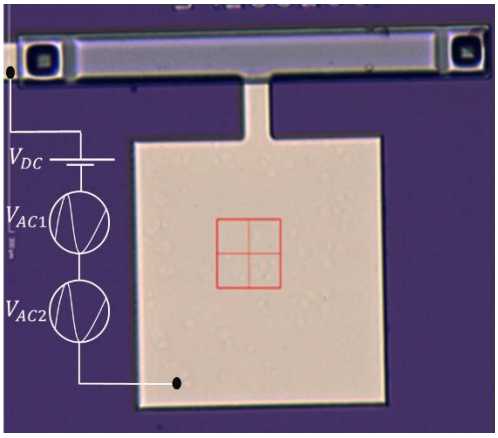

Fig. 1. Top view picture of the fabricated $600\mu m$ microbeam and the actuation pad.

Color	Material	Thickness	Width	Modulus of Elasticity	Density
	Silicon Wafer	$5\ mm$			
	SiO_2	$500\ \mu m$			
	Cr	$50\ nm$	$40\ \mu m$	$279\ GPa$	$7190\ Kg/m^3$
	Au	$500\ nm$		$79\ GPa$	$19300\ Kg/m^3$
	Au	$250\ nm$	$40\ \mu m$	$79\ GPa$	$19300\ Kg/m^3$
	Pi	$6\ \mu m$	$50\ \mu m$	$8.5\ GPa$	$1400\ Kg/m^3$
	Ni	$500\ nm$	$50\ \mu m$	$200\ GPa$	$8908\ Kg/m^3$

Fig. 2. Cross sectional view of the fabricated microbeam.

The clamped-clamped microbeam resonator, shown in Fig. 1, is fabricated using the in-house process [21, 22] on a 4" in silicon wafer coated with 500 nm SiO_2. A 250 nm chrome and gold layer is sputtered and patterned to form the lower electrode of the resonator. Then, a 2 µm amorphous silicon is deposited using the physical chemical vapor deposition to form the sacriftial layer. At the end of the fabrication process, this layer will be etched to release the resonator and create the air gap between the two electrodes. The upper electrode is formed by sputtering and patterning a Cr/Au/Cr layer of thicknesses 50nm/250nm/50nm, respectively. The chrome is used to enhance the adhesion properties between the gold and other materials. After that, a 6 µm polyimide layer is spun and cured at gradually increasing temperature from 110 C° to 350 C° in one hour and 30 minutes. A 500 nm nickel layer is sputtered and patterned on the polyimide surface to protect the microbeams during the reactive Ion etching. Finally, the wafer is diced and the scraficial layer is etched using XeF_2 dry etchant. When the two electrodes connected to an external excitation voltage, the resonator vibrates in the out-of-plane direction. Fig. 2 shows a picture illustrating the various layers of the fabricated resonator.

4. Characterization

In this section, we describe the experimental characterization setup used for testing the device and measuring the initial profile, gap thickness, and the out-of-plane vibration. The experiment is conducted on the $600\mu m$ length microbeam with full lower electrode configuration. The experimental setup, Fig. 3, consists of a micro system analyzer (MSA), which is a high frequency laser-Doppler vibrometer, under which the microbeam is placed to measure the vibration, data acquisition card, an amplifier to provide actuation signals of wide range of frequencies and amplitudes, and a vacuum chamber equipped with ports to pass the actuation signal and measure the pressure. Also, the chamber is connected to a vacuum pump that reduces the pressure as low as $4mTorr$.

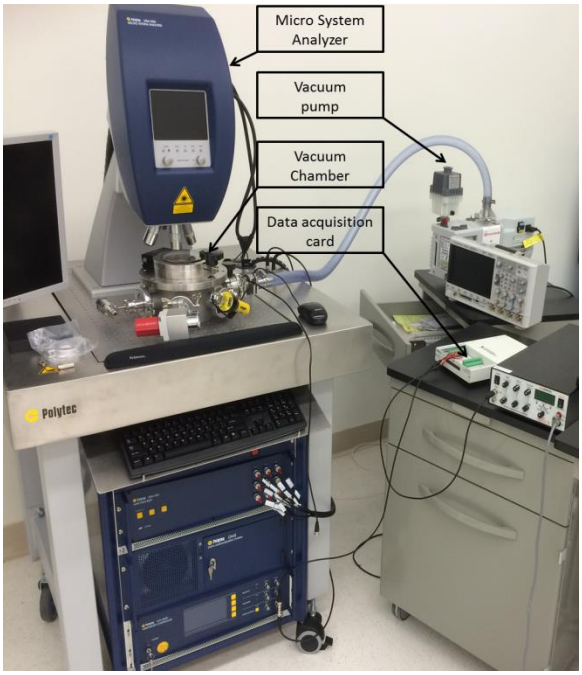

Fig. 3. Experimental setup used for testing the MEMS devices.

The microbeam is excited using the data acquisition card and the vibration is detected using the MSA. The excitation signal is composed of two AC signals V_{AC1} and V_{AC2} superimposed to a DC signal V_{DC}. The frequency response curve is generated by taking the steady state maximum amplitude of the motion $W_{\max}$.

5. Frequency response curves

Next, we demonstrate broadening of the high-amplitude response near resonance through multifrequency excitation. The generated frequency response curves near the first mode (87kHz) are depicted in Fig. 4. Each curve shows the frequency response for different values of V_{AC2}. The results are obtained by sweeping the frequency of the first AC source Ω_1 around the first mode and fixing the second source frequency Ω_2 at $500Hz$. The swept source voltage V_{AC1} and the DC voltage are

fixed at $5V$ and $5V$, respectively. The chamber pressure is fixed at $4mTorr$. Fig. 4 demonstrates clearly the enlargement of the response around the primary resonance. As shown, increasing the fixed source voltage enhances the amplitudes of the additive $(\Omega_1+\Omega_2)$ and subtractive $(\Omega_1-\Omega_2)$ resonances. These resonances arise due to the quadratic nonlinearity of the electrostatic force and the cubic nonlinearity due to mid-plane stretching. The effect of changing the fixed frequency Ω_2 on the response is illustrated in Fig. 5. As Ω_2 decreases the two resonances get closer and a continuous high amplitude band is formed. Also, the excited combination resonances can be easily tuned by properly selecting the value of Ω_2 in the LabVIEW program.

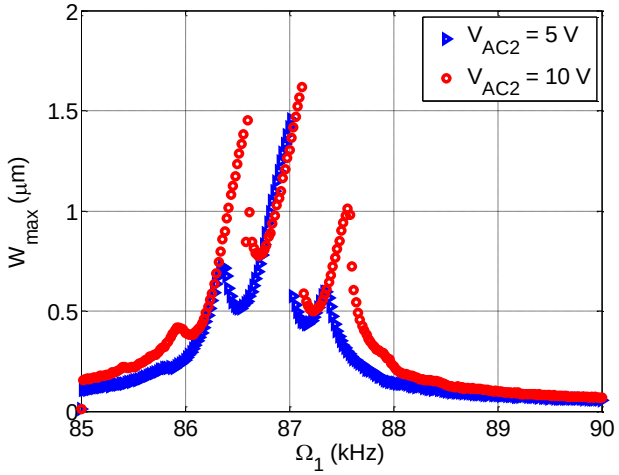

Fig. 4. Frequency response curve near the first mode of vibration for $V_{DC}=5V$, $V_{AC1}=5V$, and $\Omega_2=500Hz$.

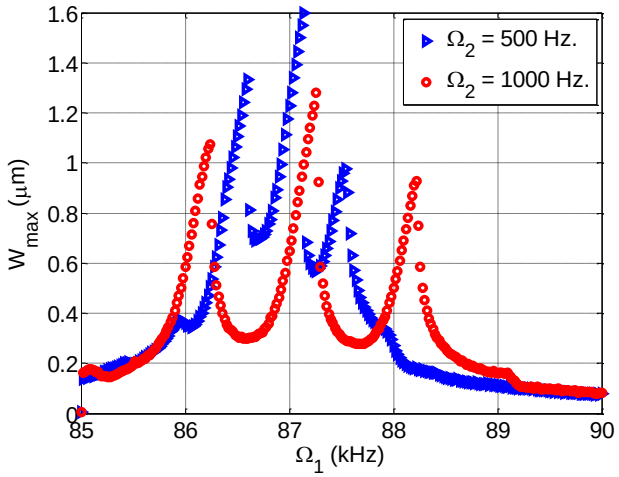

Fig. 5. Frequency response curve for different values of Ω_2 at $V_{DC}=5V$, $V_{AC1}=5V$, and $V_{AC2}=5V$ near the first mode of vibration.

Fig. 6 highlights the effect of multifrequency excitation near the third mode (355kHz) where resonance peaks of additive type at $(\Omega_1+\Omega_2)$, $(\Omega_1+2\Omega_2)$, $(\Omega_1+3\Omega_2)$ and subtractive type at $(\Omega_1-\Omega_2)$, $(\Omega_1-2\Omega_2)$, $(\Omega_1-3\Omega_2)$ are excited due to the

cubic and quadratic nonlinearities coming from mid-plane stretching and the electrostatic force, respectively. As Ω_2 decreases, these resonances merge into a high amplitude peak near the primary resonance. In addition, a hardening behavior due to the cubic nonlinearity is reported near the first and third modes of vibration.

For practical applications, where broadening of the bandwidth of resonators is required; the resonators need to operate in the linear regime. This can be ensured by optimizing the response of the resonator first to a single AC excitation to be linear, i.e., adjusting the AC and DC loads, controlling damping if possible, etc. Once a linear response is generated for a single harmonic excitation; a second source of excitation can be added. The response due to this mixing will follow qualitatively the same behavior as the response to a single excitation; if the latter is linear, the former will be most likely linear. An exception of this is for the case when the second frequency source, Ω_2, is too small, making the secondary resonances merging with the primary resonance. This can lead to significant amplification of the response. In such cases, care must be taken since this amplification might lead to a nonlinear response, and may lead to even dynamic pull-in.

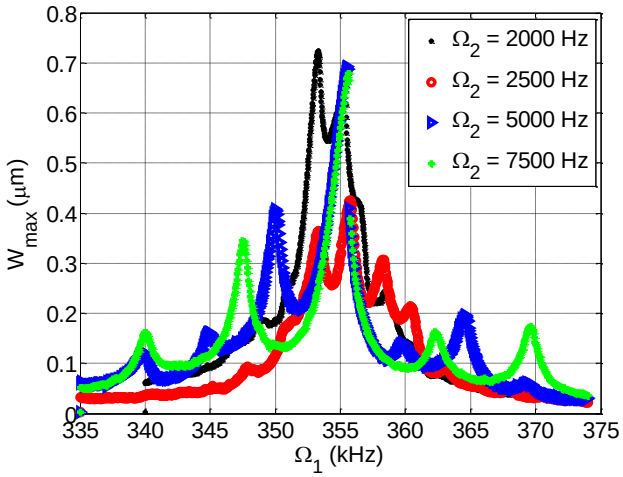

Fig. 6. Frequency response curve for different values of Ω_2 at $V_{DC} = 50V$, $V_{AC1} = 25V$, and $V_{AC2} = 40V$ near the third mode of vibration.

6. Conclusions

This demonstrates that multifrequency excitation can be used to broaden the large amplitude response around the main resonance, and hence increases the bandwidth, even for higher order modes, which can have several practical applications. Typically resonators of resonant sensors may not be driven necessary at the exact sharp peak due to temperature fluctuation, noise, and other uncertainty, which results in significant losses, lower sensitivity, and weak signal to noise ratio. The above

results prove the ability to control the resonator bandwidth by properly tuning the excitation voltage frequencies. Also, by properly tuning the excitation amplitude and frequencies, the higher order modes of vibration are triggered with high amplitudes above the noise level. These capabilities of exciting multiple resonance peak over a wide frequency band with ability to control its amplitude and location can have a promising application in increasing the resonator band width for applications, such as mixing/filtering, and mechanical logic circuits. The approach can be also promising for energy harvesting, where the resonator is excited electrically by a weak electrical signal (in principle should consumes no or little power) while the second excitation source comes from the ambient vibration. This widens the band at which the harvested energy is maximum. However, such approach needs to be further studied to verify its efficiency. In addition, actuating the resonator with multiple AC sources opens the door of multifrequncy/multiband MEMS based filters.

7. Appendix

The nondimensional equation of motion of a microbeam which is electrostatically actuated by two AC harmonic loads V_{AC1} and V_{AC2} of frequencies Ω_1 and Ω_2, respectively, superimposed to a DC load V_{DC} can be written as [18]

$$\frac{\partial^4 w}{\partial x^4}+\frac{\partial^2 w}{\partial x^2}+c_{non}\frac{\partial w}{\partial t}=\frac{\partial^2 w}{\partial x^2}\left(N_{non}+\alpha_1\int_0^1\left(\frac{\partial w}{\partial x}\right)^2 dx\right)+\frac{\alpha_2\left[V_{DC}+V_{AC1}cos\left(\Omega_1 t\right)+V_{AC2}cos\left(\Omega_2 t\right)\right]^2}{\left(1-w\right)^2} \tag{12}$$

with the normalized boundary conditions are

$$w(0,t)=0 \qquad \frac{\partial w}{\partial x}(0,t)=0$$

$$w(1,t)=0 \qquad \frac{\partial w}{\partial x}(1,t)=0 \tag{13}$$

where the nondimensional parameter in Eq. (12) are defined as

$$c_{non}=\frac{12cl^4}{ETbh^3};\alpha_1=6\left(\frac{d}{h}\right)^2;\alpha_2=\frac{6\varepsilon l^4}{Eh^3d^3};N_{non}=\frac{12Nl^2}{Ebh^3} \tag{14}$$

Where E is the modulus of elasticity, I is the moment of inertia, c is the damping coefficient, A is the cross-sectional area, ρ is the density, ε is the air permittivity, d is the air gap thickness, t is the time, x is the position along the beam, N is the axial force, b is the beam width, h is the beam thickness, l is the beam length, and w is the microbeam deflection. T is the time scale defined as

$$T = \sqrt{\frac{\rho b h l^4}{EI}} \tag{15}$$

The undamped and unactuated eigen value problem of Eq. (12) is defined as [11]

$$\phi^{(4)}(x) - N_{non}\phi^{(2)}(x) - \omega_{non}{}^2\phi(x) = 0 \tag{16}$$

To find the mode shape function $\phi_i(x)$, we solve the eigen value problem Eq. (16) for different values of the nondimensional axial force N_{non} to match the ratio of experimentally measured resonance frequencies with the nondimensional frequencies $\omega_{non3}/\omega_{non1}$ [23]. Both ratios are matched for N_{non}=41.9. The axial force arises due to the residual stress from depositing the different layers at extremely different temperatures.

In previous work [23], we found $EI = 1.06\times10^{-10}$ for a 400 µm long microbeam. The value of *EI* is extracted by measuring the static deflection of a 400 clamped-clamped microbeam subjected to a gradually increasing DC voltage. Then, the static deflection equation is solved for different values of *EI* until the experimental and simulation results are matched. We assumed that beams with the same cross section and fabricated from the same material, but different length will have the same *EI* value. The nondimensional damping c_{non} is extracted by solving the dynamical equation and matching the simulation and experimental results.

Equation (12) is solved using three modes in the Galerkin approximation. The simulation and experimental results near the first mode is shown in Fig.7 where a qualitative agreement can be noticed. The discrepancies in the results can be attributed to fabrication imperfection and the use of three modes in the Galerkin approximation.

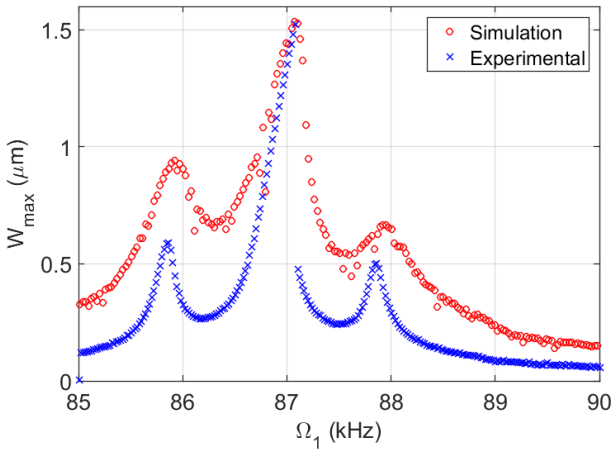

Fig. 7. Simulation and Experimental result of the microbeam near the first mode V_{DC} = 5V, V_{AC1} = 5V, V_{AC2} = 5V, and Ω_2 = 1 kHz.

8. References

[1] C. Acar, A. Shkel, MEMS vibratory gyroscopes: structural approaches to improve robustness, Springer Science & Business Media, 2008.

[2] D. Zhu, M.J. Tudor, S.P. Beeby, Strategies for increasing the operating frequency range of vibration energy harvesters: a review, Measurement Science and Technology, 21 (2010) 022001.

[3] R. Harne, K. Wang, A review of the recent research on vibration energy harvesting via bistable systems, Smart Materials and Structures, 22 (2013) 023001.

[4] J.F. Rhoads, S.W. Shaw, K.L. Turner, R. Baskaran, Tunable microelectromechanical filters that exploit parametric resonance, Journal of Vibration and Acoustics, 127 (2005) 423-430.

[5] H.-T. Kim, J.-H. Park, Y.-K. Kim, Y. Kwon, Low-loss and compact V-band MEMS-based analog tunable bandpass filters, Microwave and Wireless Components Letters, IEEE, 12 (2002) 432-434.

[6] A. Abbaspour-Tamijani, L. Dussopt, G.M. Rebeiz, Miniature and tunable filters using MEMS capacitors, Microwave Theory and Techniques, IEEE Transactions on, 51 (2003) 1878-1885.

[7] D.N. Guerra, A.R. Bulsara, W.L. Ditto, S. Sinha, K. Murali, P. Mohanty, A noise-assisted reprogrammable nanomechanical logic gate, Nano letters, 10 (2010) 1168-1171.

[8] I. Mahboob, E. Flurin, K. Nishiguchi, A. Fujiwara, H. Yamaguchi, Interconnect-free parallel logic circuits in a single mechanical resonator, Nature communications, 2 (2011) 198.

[9] D. Hatanaka, I. Mahboob, H. Okamoto, K. Onomitsu, H. Yamaguchi, An electromechanical membrane resonator, Applied Physics Letters, 101 (2012) 063102.

[10] G.A. Steele, A.K. Hüttel, B. Witkamp, M. Poot, H.B. Meerwaldt, L.P. Kouwenhoven, H.S. van der Zant, Strong coupling between single-electron tunneling and nanomechanical motion, Science, 325 (2009) 1103-1107.

[11] M.I. Younis, MEMS Linear and Nonlinear Statics and Dynamic, Springer Science & Business Media, 2011.

[12] K.B. Lee, L. Lin, Y.-H. Cho, A closed-form approach for frequency tunable comb resonators with curved finger contour, Sensors and Actuators A: Physical, 141 (2008) 523-529.

[13] G. Piazza, P.J. Stephanou, A.P. Pisano, Single-chip multiple-frequency ALN MEMS filters based on contour-mode piezoelectric resonators, Journal of Microelectromechanical Systems, 16 (2007) 319-328.

[14] E. Mastropaolo, I. Gual, R. Cheung, Silicon carbide electrothermal mixer-filters, Electronics letters, 46 (2010) 62-63.

[15] H. Cho, M.-F. Yu, A.F. Vakakis, L.A. Bergman, D.M. McFarland, Tunable, broadband nonlinear nanomechanical resonator, Nano letters, 10 (2010) 1793-1798.

[16] S. Ilyas, A. Ramini, A. Arevalo, M. Younis, An Experimental and Theoretical Investigation of a Micromirror Under Mixed-Frequency Excitation.

[17] A. Ramini, M.I. Younis, Q.T. Su, A low-g electrostatically actuated resonant switch, Smart Materials and Structures, 22 (2013) 025006.

[18] M. Younis, Multi-mode excitation of a clamped–clamped microbeam resonator, Nonlinear Dynamics, 80 (2015) 1531-1541.

[19] M. Younis, A. Nayfeh, A study of the nonlinear response of a resonant microbeam to an electric actuation, Nonlinear Dynamics, 31 (2003) 91-117.

[20] A. H. Nayfeh and D. Mook, *Nonlinear Oscillations*, John Willey and Sons, New York, 1979.

[21] L. Marnat, A.A. Carreno, D. Conchouso, M.G. Martinez, I.G. Foulds, A. Shamim, New Movable Plate for Efficient Millimeter Wave Vertical on-Chip Antenna, IEEE Transactions on Antennas and Propagation, 61 (2013) 1608-1615.

[22] A. Alfadhel, A.A. Arevalo Carreno, I.G. Foulds, J. Kosel, Three-Axis Magnetic Field Induction Sensor Realized on Buckled Cantilever Plate, IEEE Transactions on Magnetics, 49 (2013) 4144-4147.

[23] N. Jaber, A. Ramini, A.A. Carreno, M.I. Younis, Higher order modes excitation of electrostatically actuated clamped–clamped microbeams: experimental and analytical investigation, Journal of Micromechanics and Microengineering, 26 (2016) 025008.

Nizar Jaber received a B.S. degree in Mechanical Engineering from Jordan University of Sciences and Technology, Jordan in 2010. He earned his Masters in Mechanical Engineering from King Abdullah University of Science and Technology (KAUST) in 2013. He is currently enrolled as a PhD student in Mechanical Engineering in KAUST. His research interests include linear and nonlinear dynamics of MEMS based resonators with their applications in MEMS sensors and actuators. He is a student member of American Society of Mechanical Engineers (ASME).

Abdallah Ramini was born in Amman, Jordan, in 1981. He received the Bachelor's and Master's degrees in mechatronics engineering from the Jordan University of Science and Technology, Irbid, Jordan, in 2004 and 2007, respectively, and the Ph.D. degree in mechanical engineering from the Binghamton State University of New York (SUNY), Binghamton, NY, USA, in 2012, with a focus on the static and dynamic behaviors of MEMS devices and structures under shock. From 2012 to 2013, he was with SUNY as a Post-Doctoral Fellow working on dynamical integrity of MEMS resonators. Since 2013, he has been a Post-Doctoral Fellow with the King Abdullah University of Science and Technology, Thuwal, Saudi Arabia, where he is currently performing his research activity with the MEMS and NEMS Characterization and Motion Laboratory. His research focuses on MEMS resonant and actuator applications. He is a member of the American Society of Mechanical Engineers.

Qais Hennawi received a B.S. degree in Mechanical Engineering from Jordan University of Sciences and Technology, Jordan in 2013. He earned his Master in Mechanical Engineering from King Abdullah University of Science and Technology (KAUST) in 2014. He is currently working as a petroleum engineer in the Arabian Oil Company (ARAMCO).

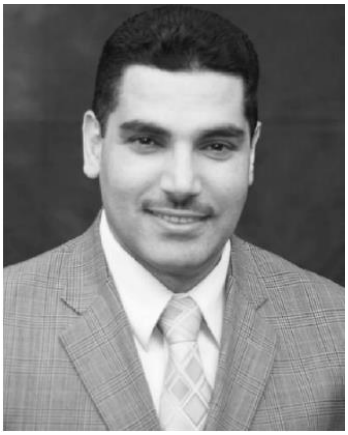

Mohammad I. Younis received the B.S. degree in mechanical engineering from the Jordan University of Science and Technology, Irbid, Jordan, in 1999, and the M.S. and Ph.D. degrees in engineering mechanics from Virginia Polytechnic Institute and State University, Blacksburg, VA, USA, in 2001 and 2004, respectively. He is currently an Associate Professor of Mechanical Engineering with the King Abdullah University of Science and Technology, Thuwal, Saudi Arabia, and the State University of New York (SUNY), Binghamton, NY, USA. He serves as the Director of the MEMS and NEMS Characterization and Motion Laboratory. Dr. Younis was a recipient of the SUNY Chancellor's Award for Excellence in Scholarship and Creative Activities in 2012, the National Science Foundation Faculty Early Career Development Award in 2009, and the Paul E. Torgersen Graduate Research Excellence Award in 2002. He holds three U.S. patents in MEMS sensors and actuators. He serves as an Associate Editor of Nonlinear Dynamics, the Journal of Computational and Nonlinear Dynamics, the Journal of Vibration and Control, and Mathematical Problems in Engineering. He has authored the book entitled MEMS Linear and Nonlinear Statics and Dynamics (Springer, 2011). He is a member of the American Society of Mechanical Engineers.